



## Journal of Advanced Research in Numerical Heat Transfer

Journal homepage:  
<https://semarakilmu.com.my/journals/index.php/arnht/index>  
ISSN: 2735-0142



# Effect of Vortex Generator Angle on Fin and Tube Heat Exchanger

Damora Rhakasywi<sup>1</sup>, Abdul Wasito<sup>1</sup>, Elang Pramudya Wijaya<sup>1</sup>, Reda Rizal<sup>2</sup>, Dendy Adanta<sup>3,\*</sup>

<sup>1</sup> Mechanical Engineering, Faculty of Engineering, Universitas Pembangunan Nasional Veteran Jakarta, Pondok Labu, Jakarta, 12450, Indonesia

<sup>2</sup> Faculty of Engineering, Industrial Engineering, Universitas Pembangunan Nasional Veteran Jakarta, Pondok Labu, Jakarta, 12450, Indonesia

<sup>3</sup> Department of Mechanical Engineering, Faculty of Engineering, Universitas Sriwijaya, Indralaya, 30662, South Sumatera Indonesia

### ARTICLE INFO

### ABSTRACT

#### Article history:

Received 12 October 2023

Received in revised form 11 November 2023

Accepted 10 December 2023

Available online 31 January 2024

#### Keywords:

Vortex generator; CFD; fin and tube

In refrigeration systems, a common installed component is the fin and tube heat exchanger. The fluid that passes through the fins has lower thermal conductivity than the fluid flowing inside the tubes, resulting in high thermal resistance. To address this problem, a vortex generator was introduced in the design of the fin and tube heat exchanger. This passive approach aims to improve heat transfer within heat exchangers by promoting the mixing of hot and cold fluids, thereby improving the convection coefficient. This study seeks to investigate the impact of the longitudinal vortex on pressure drop and the increase in the convection coefficient. Through numerical simulations, the study examined seven rows of tubes at angles of attack of 5°, 10°, and 15°. The vortex generator that used in this study are rectangular winglet pairs (RWP), concave rectangular winglet pairs (CRWP), and convex rectangular winglet pairs (CRWP). It was concluded that using Concave Rectangular Winglet Pairs (CRWP) as the vortex generator shape at a 15° angle of attack led to the highest difference in convection coefficient, reaching 154.13% of the baseline case with a Reynolds value of 662. Furthermore, the use of a Rectangular Winglet Pairs (RWP) vortex generator at a 5° angle of attack and a Reynolds value of 284 resulted in the least impact on pressure drop, with an increase of 45.29% compared to the baseline case.

## 1. Introduction

Installing vortex generators was an innovation to increase the heat transfer on a heat exchanger. A heat exchanger is a tool used to transfer heat between two fluids kept apart by a solid barrier and operating at different temperatures [1]. Several applications of heat exchangers as heat exchange devices can be found in industries related to air conditioning, power generation, waste gas utilization systems, and chemical processing systems. One of the most widely used varieties in air conditioning is fin and tube heat exchanger, where the airflow passes through the fin and the heat transfer from the tube that is connected to the fin [2]. There is a significant level of thermal resistance in the airflow through the fin section. The convective heat transfer coefficient is low when it encounters high thermal resistance [3]. Thus, it is necessary to decrease thermal resistance by modifying the fin's grid

\* Corresponding author.

E-mail address: [dendyadanta@gmail.com](mailto:dendyadanta@gmail.com) (Dendy Adanta)

<https://doi.org/10.37934/arnht.16.1.8299>

structure to increase the coefficient. Furthermore, this modification causes the flow's pressure drop to increase [4,5].

A study suggests that modifying the fin by adding protrusions to the surface used in the heat exchanger aims to enhance the overall heat transfer performance [6]. These surface protrusions come in various shapes, including plain, wavy, louver, slit, offset, and others [7]. Protrusion modification is a passive method that generating vortex on fin surface, this method could increase heat transfer [8].

A passive technique that can create vortices and swirling flow patterns is a vortex generator (VG). Vortex generators come in two varieties: delta and rectangular, which are applied by pressing, welding, or molding. Vortex generators can produce two different kinds of vortices: transverse (TVG) and longitudinal (LVG) [4]. Since transverse vortices are mainly concentrated on the wake side of the vortex generator, they are less effective than longitudinal vortices. Heat propagation therefore only happens in that particular area [9]. In this period, longitudinal vortices set off a subsequent flow that results in unstable flow and interferes with the development of thermal boundary layers. An unstable flow produces high-scale turbulence [10].

Studies [11] have been studied the effect vortex generators in enhancing the heat transfer, with variations in their placement, shape, and orientation. Numerical research of the thermal and fluid characteristics of pin-fin type heat sinks using delta winglet vortex generators has shown that a decrease in thermal resistance is attributed to an increase in Reynolds number and a high winglet angle of attack at 30 degrees with a common flow up arrangement [12]. Furthermore, research on the use of curved vortex generators in fin-tube heat exchangers has shown that the flow intensity is greater when using a larger radius for the curvature of the applied vortex generator in the fin-tube heat exchanger. The vortex generator with a central angle ( $\theta$ ) = 25°, an angle of attack ( $\beta$ ) = 15°, and an overall performance factor (R) = 1,06 exhibits the most optimum thermal and hydraulic performance [13]. Research involving variations in winglet shapes, specifically concave and convex curved vortex generators, has shown that the concave curved vortex generator enhances heat transfer better. It resulted in an 11.3% increase in the surface goodness factor ((JF) at Re = 1400,  $\beta$  = 20°, dan  $\theta$  = 80°, compared to the convex curved vortex generator [14].

This research was conducted numerically based on experiments conducted on the evaporator created by Joardar *et al.*, [15]. With angle of attack variations of 5°, 10°, and 15°, the rectangular winglet pair (RWP) and the baseline are replaced by the concave rectangular winglet pair (CRWP) and convex rectangular winglet pair (CxRWP) of VG. The earlier study is still relevant to the research utilizing CRWP and CxRWP. Therefore, the goal of this study is to enhance the pressure drop and convective heat transfer through modifying both the type and angle of VG on the fin-tube heat exchanger.

## 2. Methodology

### 2.1 Heat Exchanger Geometry and Boundary Conditions

To analyze the influence of varied vortex generator shapes and angles of attack on fin and tube heat exchangers and their effects on flow velocity distribution, convection coefficient, temperature distribution, and pressure drop. Since the higher temperature of air flow in the inlet side than the flow on the tube side, the heat will transfer through convection. It is anticipated that vortex generators will create swirling flow patterns that prevent thermal boundary layers from forming, increasing the convection coefficient for heat transfer. The research's problem statement is depicted in Figure 1 below.

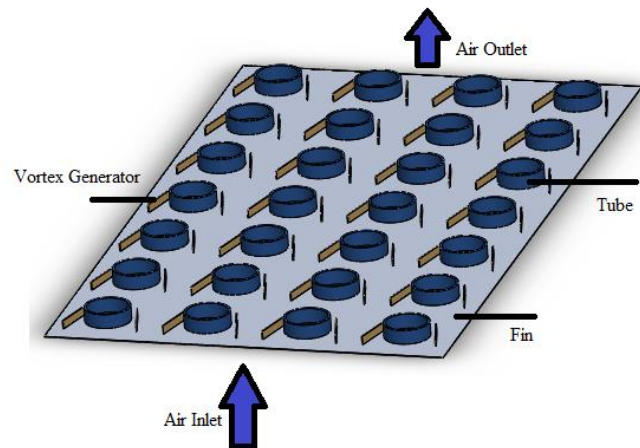


**Fig. 1.** VG Fin-Tube heat exchanger

The heat exchanger's geometry consists of circular tubes arranged in an inline, or parallel, tube configuration, along with plain fins. The model's dimensions are displayed in Figure 2 below.

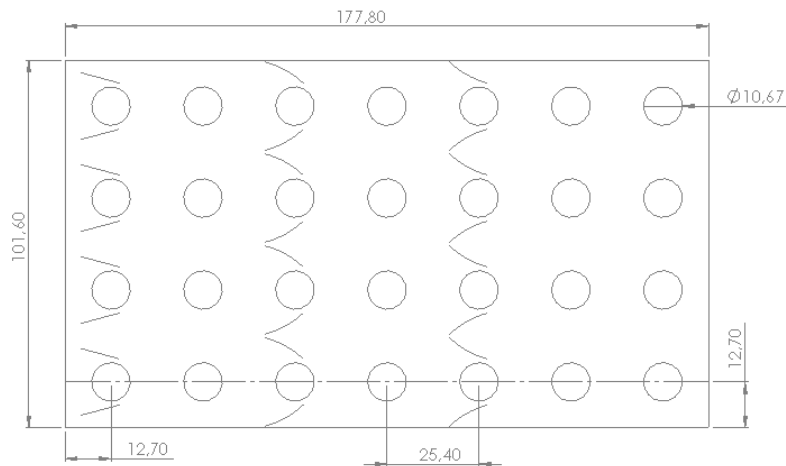


**Fig. 2.** Heat exchanger dimension

Each fin's length and width are shown to be 177.88 mm and 101.6 mm, respectively. As can be seen in Figure 2 above, the tube diameter is 10.67 mm, the length between the tubes' center points is 25.4 mm, also the length between the first tube's center point and the wall in both horizontal and vertical directions is 12.7 mm.

The material used for the heat exchanger and the added vortex generator is aluminum with specifications as listed in Table 1.

**Table 1**  
 Aluminium specification

Properties	Value
Density	2719 kg/m <sup>3</sup>
Specific heat	871 J/kg.K
Thermal conductivity	202,4 W/m.K

The modeling of the air flow inlet involves varying its velocity with Reynolds numbers ranging from 284 to 662 at a temperature of 310.6 K, while the tube temperature remains constant at 291.77 K. Further specifications of the inlet fluid are provided in Table 2 below.

**Table 2**  
 Fluid specification

Properties	Value
Density	1,13618 kg/m <sup>3</sup>
Specific heat	1007 J/kg.K
Thermal conductivity	0,0264313 W/m.K
Dynamic viscosity	1,90627 x 10 <sup>-5</sup> kg/m.s

The dimensions of the vortex generator geometry used in this research, which is varied with rectangular winglet by figure (a), concave rectangular winglet (figure (b)), and convex rectangular winglet (figure (c)), are shown in Figure 3 below.

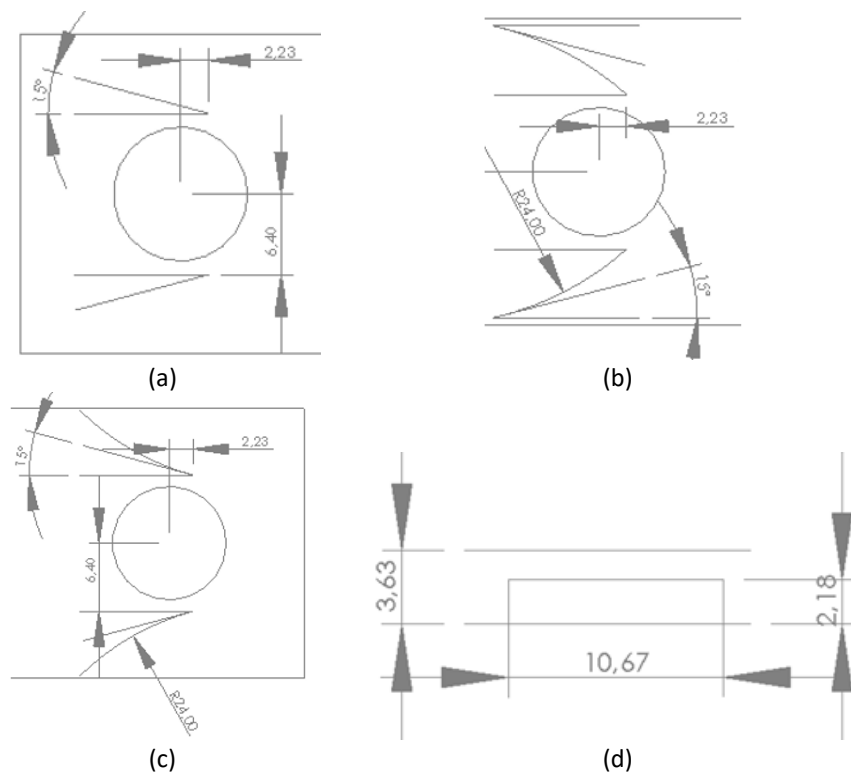


**Fig. 3.** Vortex generators type (a) Rectangular (b) Concave (c) Convex (d) Front View (in mm) [15]

It is shown that the length between the trailing edge of VG and the centre point of the tube is varied 6.4 mm and 2.23 mm. Moreover, in this study, the height of the VG is 60% of the tube height for concave and convex VG, and the radius of curvature is set at 24 mm. The VG used in this study had three different angles of attack: 5°, 10°, and 15°. Figure 3 (a), (b), and (c) shows where the VG is positioned on the fin. In this study, seven rows of VGs were used. Table 3 shows the boundary condition.

**Table 3**

Boundary condition

Boundary condition	Detail
Inlet	Velocity inlet 0,75 m/s – 1,75 m/s 310,6 K
Outlet	Outflow
Tube wall	Stationary wall 291,77 K
VG dan Fin	Stationary Wall No Slip

## 2.2 Governing Equation

In every calculation that analyzes fluid flow, transient simulation was used. ANSYS Fluent 19.2 was used to perform the simulation. These equations are derived from Newton's Second Law applied to fluid dynamics and the heat equation, which involves heat transfer within the fluid. The governing equations used to solve this simulation, which consists of the continuity, momentum, and energy equation, can be formulated using the Gauss theorem [16].

$$\frac{\partial \rho}{\partial t} = -\nabla \cdot (\rho \vec{u}) \quad (1)$$

where  $\rho$  is fluid density and  $\vec{u}$  is velocity vector.

$$\frac{\partial \rho \vec{u}}{\partial t} + \nabla \cdot (\rho \vec{u} \vec{u}) = -\nabla p + \rho \vec{g} + \nabla \cdot (\mu \nabla \vec{u}) \quad (2)$$

where  $p$  is static pressure,  $\vec{g}$  is gravitational force, and  $\mu$  is kinematic viscosity.

$$\frac{\partial \rho H}{\partial t} + \nabla \cdot (\rho \vec{u} H) = \nabla \cdot (k \nabla T) \quad (3)$$

where  $H$  is entalpy,  $k$  is fluid thermal conductivity, and  $T$  is fluid temperature.

The calculation of pressure in CFD simulations can be performed using the momentum conservation equation, as shown in Eq. (4) below [17].

$$\frac{\partial}{\partial t} (\rho \vec{v}) + \nabla \cdot (\rho \vec{v} \vec{v}) = -\nabla p + \nabla \cdot (\bar{\tau}) + \rho \vec{g} + \vec{F} \quad (4)$$

where  $\bar{\tau}$  is tensor strain,  $\rho \vec{g}$  is the body force affected by gravitation, dan  $\vec{F}$  is external body force. The calculation of heat transfer in CFD simulations can be performed using the energy conservation equation, as shown in Eq. (5) below [17].

$$\frac{\partial}{\partial t} (\rho E) + \nabla \cdot (\vec{v} (\rho E + p)) = \nabla \cdot \left( k_{eff} \nabla T - \sum_j h_j \vec{J}_j + (\bar{\tau}_{eff} \cdot \vec{v}) \right) + S_h \quad (5)$$

where  $K_{eff}$  effective conductivity,  $\vec{J}_j$  is flux diffusion species  $j$ , dan  $S_h$  is heat from chemical reaction and volumetric heat source. With  $E$ ,  $h$ , dan  $h_j$  on the Eq. (6) to (8).

$$E = h - \frac{p}{\rho} + \frac{v^2}{2} \quad (6)$$

$$h = \sum_j Y_j h_j + \frac{p}{\rho} \quad (7)$$

$$h_j = \int_{T_{ref}}^T c_{p,j} dT \quad (8)$$

where  $Y_j$  is mass fraction species,  $T_{ref}$  depends on model and the solver used. in pressure-based solver, the value of  $T_{ref}$  is 298.15 K and in density-based solver the  $T_{ref}$  is 0 K.

### 2.3 Simulation Setup

3D model of the vortex generators was modelled by SOLIDWORKS, it can be seen in Figure 4 below. Different variation of the angle of attack in each VG is arranged in a common flow up configuration. The VG type is varied to rectangular, concave and convex.

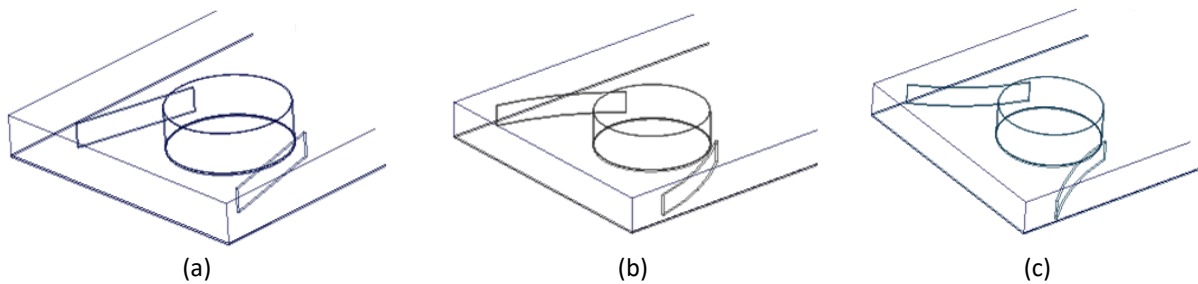


**Fig. 4.** Geometry: (a) Rectangular, (b) Concave, and (c) Convex

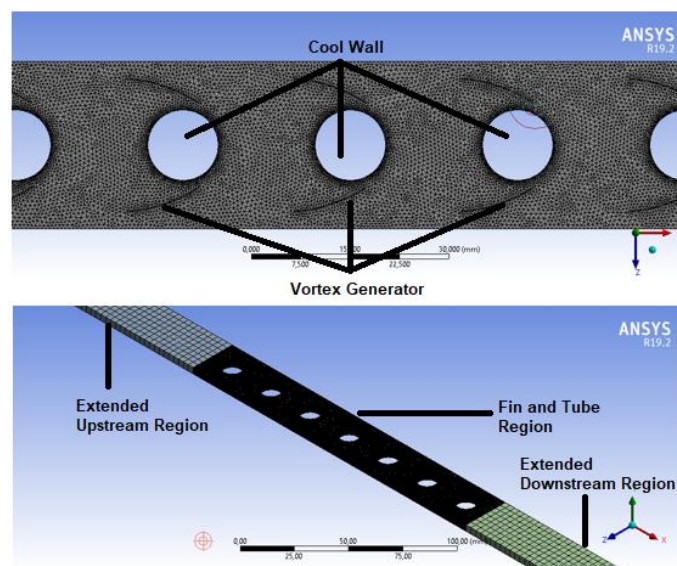


**Fig. 5.** Computational domain

A computational domain and mesh can be seen in Figure 5 and is separated into the fin and tube region, and the extended upstream and downstream region. To ensure that the fluid flow ends up in a fully developed manner, and geometry extension has been made as an extended air inlet area. Along the upstream and downstream regions, where vortex generators and tubes are applied, is the

fin and tube region. Additionally, the extended downstream region is used to stop any backflow of fluid as it leaves the domain.

### 2.4 Mesh Independency

Once the simulation modeling has been determined, the next step is meshing, which involves creating small elements, each with values for a given simulation. Mesh quality significantly affects the simulation results and can be optimized by considering the device's hardware capabilities and the iteration processing time to obtain results with the highest possible accuracy.

The tetrahedral method is used in the fin and tube region domain to achieve maximum accuracy due to its complex geometry. Figure 6 below shows the detail of the mesh for one of the models.

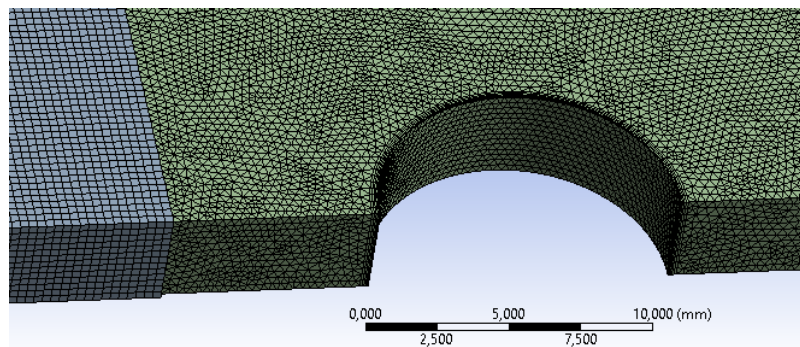


Fig. 6. Meshing

In addition, Table 4 below summarizes the number of nodes, elements, and mesh quality values, including skewness, for each modeling variation using the same parameters as in Table 3.

**Table 4**  
 Skewness of mesh

Configuration	Angle of attack	Nodes	Elements	Maximum skewness
Without vortex generator		210.645	1.076.522	0,8458
Rectangular winglet	5°	220.500	1.119.836	0,8497
	10°	221.192	1.123.222	0,842
Concave rectangular winglet	15°	221.870	1.127.551	0,8466
	5°	222.947	1.132.364	0,8475
	10°	294.411	1.228.512	0,84
Convex rectangular winglet	15°	224.280	1.137.088	0,8490
	5°	222.102	1.127.949	0,8467
	10°	223.186	1.133.408	0,8451
	15°	223.609	1.133.658	0,8491

Based on the previously mentioned Table 4, the mesh used in each variation of this research modelling fulfil the standards. This is because the maximum skewness values are within an acceptable range, as per the standards by Ansys UK Ltd, as shown in Figure 7 below.



Fig. 7. Skewness mesh metrics spectrum [17]

### 3. Results and Discussion

#### 3.1 Mesh Independence Test

Mesh independence study is conducted to decide the type and number of elements that will be used to meet the criteria and numerical accuracy. The study is to overcome the save the computational time while still managing the simulation quality. The mesh independence was using Richardson extrapolation, to reduce the computing time without sacrificing the simulation quality [18,19]. This is done by varying the mesh size with five different sizes, each having a different number of elements: 153,047, 250,682, 469,390, 1,119,555, and 1,756,836. The test is performed on a 10-degree concave geometry with a Reynolds number of 473.

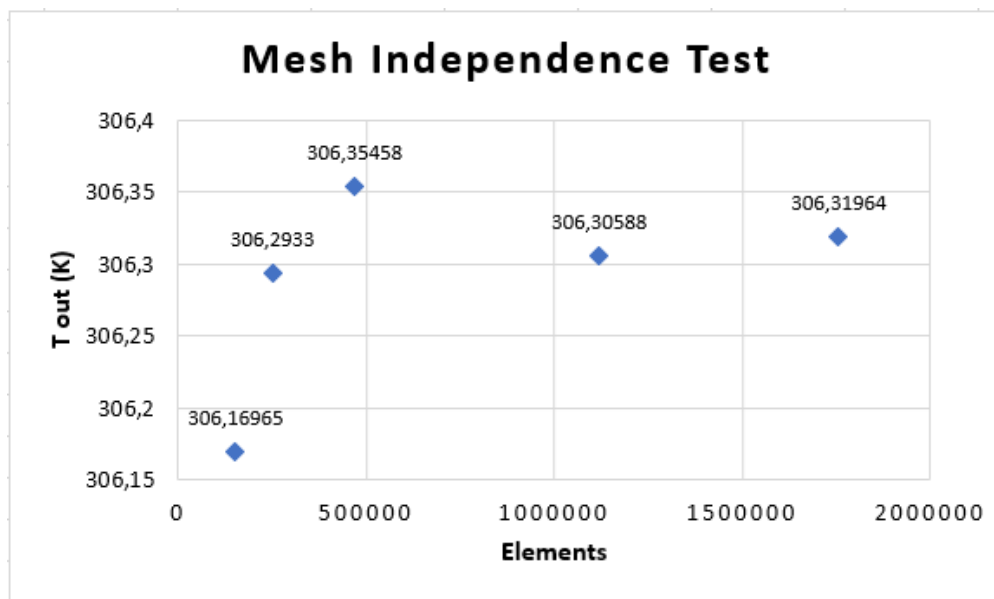
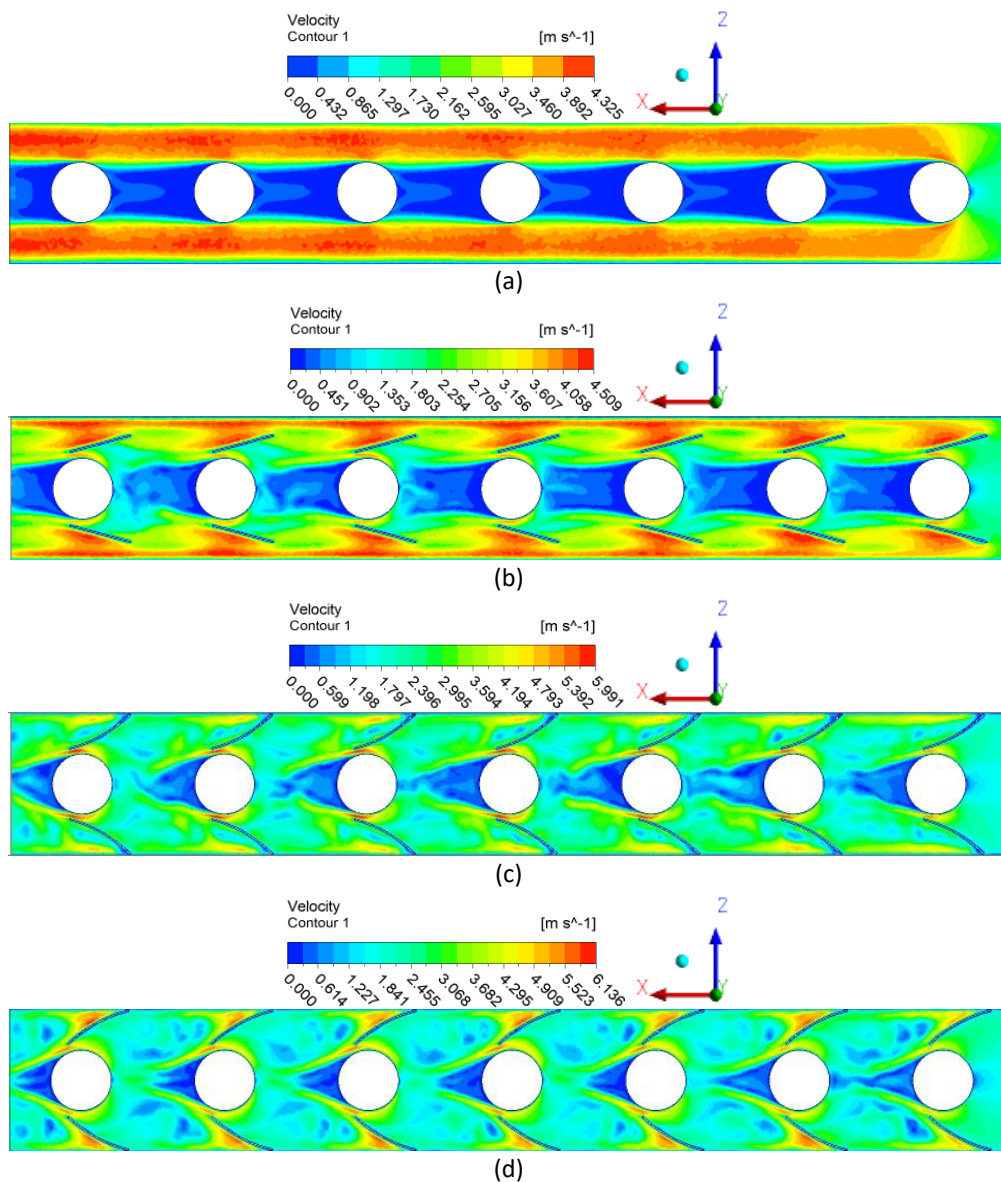


Fig. 8. Mesh independence test

The size and type of the mesh with a total of 1,119,555 elements have been selected as the mesh independence criteria, as shown by the mesh independence test graph in Figure 8. This choice was made since when the number of elements was increased, the outlet temperature at the outlet section essentially stays the same (varying by 0.004%).

#### 3.2 Vortex Generator Analysis on Velocity Distribution

The influence of the shape and angle of attack on the velocity distribution can be observed from the simulation results in the form of velocity contour plots. The simulations were performed at a Reynolds number of 662 in the positive x-axis direction. Figure 9 below compares the heat exchanger without using any vortex generator (baseline) and with the a 15° angle VG.



**Fig. 9.** Velocity contour (a) Baseline (b) RWP 15° (c) CxRWP 15° (d) CRWP 15°

In Figure 9 above, you can observe the characteristics of the airflow velocity distribution without using a vortex generator (baseline) and with various vortex generator configurations. Figure 9 (a) shows that the velocity distribution in the first to seventh rows, the separation region behind the tube, remains constant, as does the velocity around the tube. Furthermore, in Figure 9 (b), (c), and (d), it is shown that the airflow velocity (inlet) increases in the gaps between the vortex generators and the tube. This occurs because the fluid flows through a narrow cross-section. Additionally, increased angle of attack on the VG also enhances the velocity in the gap as the VG's area becomes wider, directing the flow towards the narrow gap.

Moreover, the use of various vortex generator configurations can minimize the separation region behind the tube. In Figure 9 (d), it represents the smallest separation region resulting from the use of the VG variations. The reason of the separation is the longitudinal vortex generated by the VG. It was found that the maximum velocity increased by 36.08% compared to the case of RWP 15 degrees and a Reynolds number of 662.

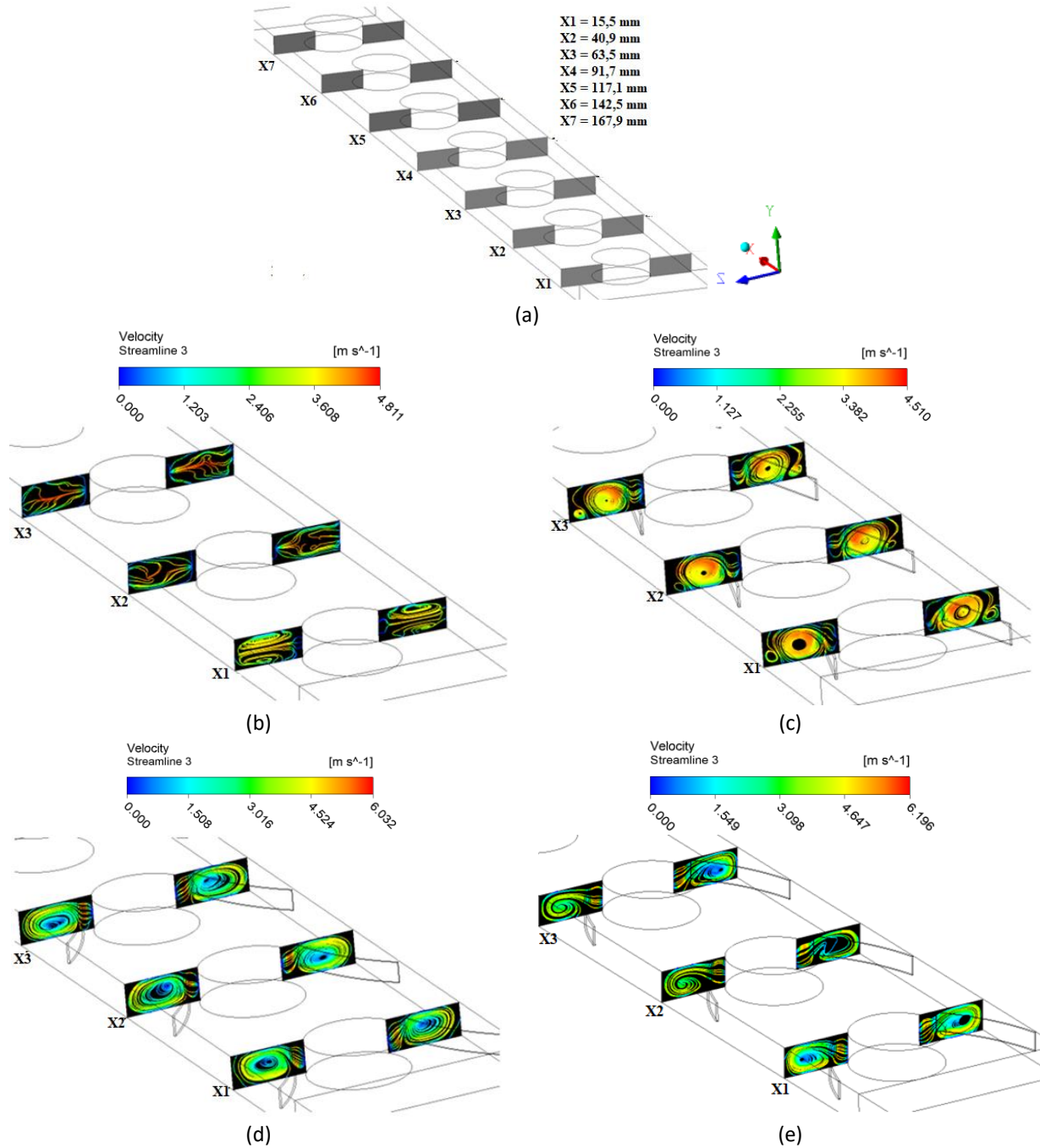


**Fig. 10.** Longitudinal vortex streamline (a) Plane, (b) Baseline, (c) RWP 15°, (d) CxRWP 15° (e) CRWP 15°

The variations in streamlines brought about by using different vortex generator configurations in the heat exchanger are shown in Figure 10. Uniform flow velocity distribution can be seen in Figure 10 (b). Nevertheless, implementing VG in the heat exchanger made the flow to rotate. It is evident from this rotational motion that longitudinal vortices formation promotes fluid direction changed between the main flow and behind the wake region of the vortex generator [20]. The rotational motion in the flow is clearly influenced by the vortex generator geometry variations, as seen in Figure 10 (c), (d), and (e). The wider frontal surface of CRWP than CxRWP and RWP results in a stronger rotational flow generated by the CRWP shape. This is also reflected in the 37.65% increase in maximum velocity compared to CxRWP and RWP. In addition, the vortex generator's common flow up orientation results in the rotation of clockwise on the right side and counterclockwise on the left

side of the vortex as it approaches the channel's center of flow. Increased heat transfer results from the disruption of the thermal boundary layers caused by both of these vortices [21].

### 3.3 Influence of Vortex Generator Variation on Flow Temperature Distribution

Figure 11 below shows the temperature contour in base case, RWP, CxRWP, and CRWP with seven pairs of vortex generators at a Reynolds number of 662 in the positive x-axis direction at a 15° angle of attack. The more uniform the temperature distribution, the more higher heat transfer on the tube wall to the working fluid.

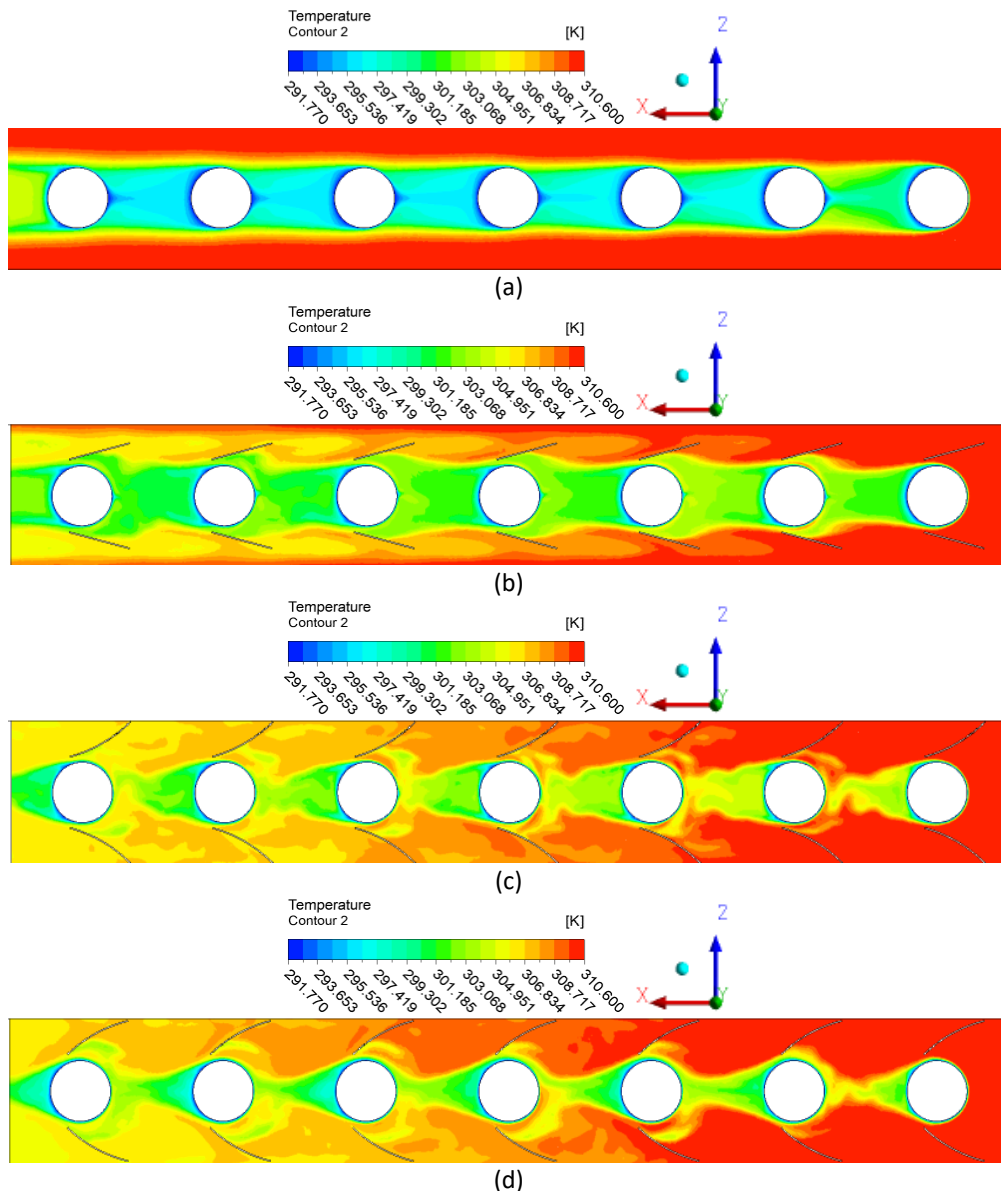


**Fig. 11.** Temperature contour (a) Baseline, (b) RWP15° (c) CxRWP 15° (d) CRWP 15°

In Figure 12, the temperature contours at the streamwise direction  $Y = 2.54$  mm shows that low temperatures occur on the backside of the tube, while high temperatures occur around the tube, which is caused by the longitudinal vortex that develops [22]. Lower temperature was developed in the wake area since the flow velocity is slower, resulted in low heat transfer. Therefore, the wake area must be minimized to increase fluid mixing to enhance heat transfer. The installation of vortex

generators creates a high temperature difference around the vortex generator, and secondary flows are induced. Subsequently, the flow mixed with the flow in the tube separation area, causing thinner thermal boundary layer occurs and significantly increasing heat transfer.

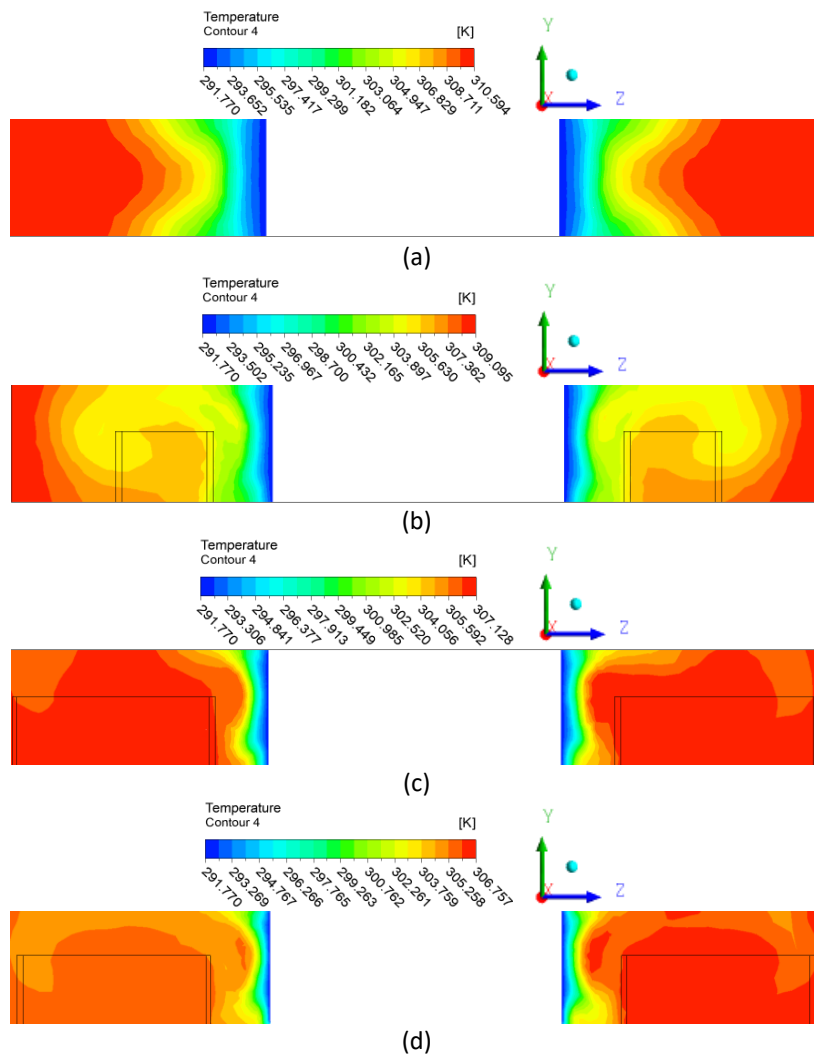


**Fig. 12.** Streamwise temperature contour  $X = 167,9$  mm (a) Baseline (b) RWP  $15^\circ$  (c) CxRWP  $15^\circ$  (d) CRWP  $15^\circ$

Figure 12 shows that low temperatures are seen near the wall tube. Vortex generators can distribute high-temperature flow from the main flow to mix with the low-temperature flow near the wall tube. In Figure 12 (a), (b), (c), and (d), the temperature contour result from the presence of longitudinal vortices is evident, increasing flow mixing and thin thermal boundary layer. In Figure 12 (d), the temperature distribution near the wall tube exhibits the thinnest thermal boundary layer and produces the best temperature distribution on the outlet side, with an improvement of 1.7699% compared to the inlet side for each variation of the vortex generator, which will affect the convection coefficient value.

### 3.4 The Vortex Generator Variations Influence on The Convective Heat Transfer Coefficient

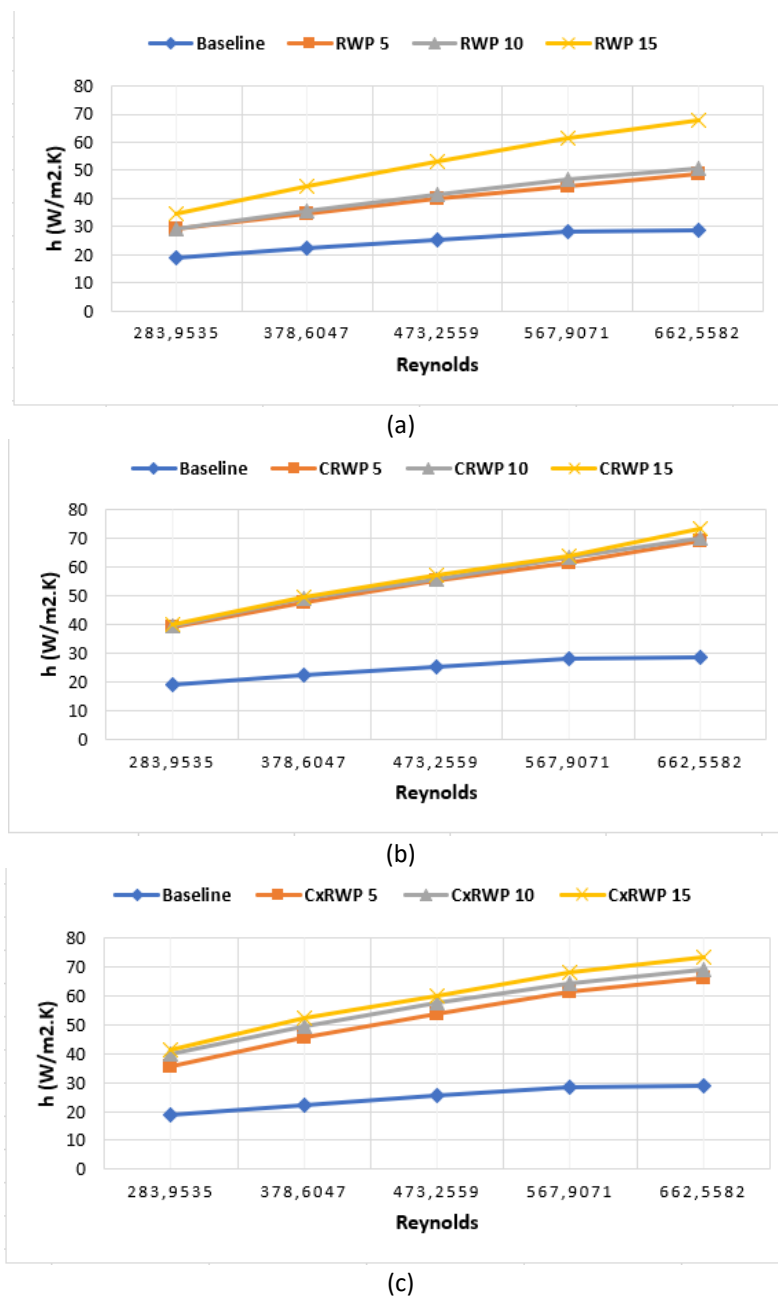


Fig. 13. Convection coefficient graph (a) RWP (b) CRWP (c) CxRWP

$$h = \frac{q_{con}}{AT \cdot \Delta T_{lm}} \quad (9)$$

Heat transfer calculation was obtained using Eq. (9). The vortices generated by the VG at high flow velocities resulted in a stronger vortex flow formation compared to low flow velocities [10]. The CRWP vortex generators shows a higher increment in the convective heat transfer coefficient compared to CxRWP and RWP VG due to the larger contact area [23].

When the 5° angle of attack and the value of Reynolds number is 662, there is slight increase in the convective heat transfer coefficient in RWP, CxRWP, and CRWP vortex generator by 68.57%, 129.97%, and 139.36%, compared to the case without VG (refer to Figure 13). Furthermore, the 10° case with Reynolds number 662 of RWP, CxRWP, and CRWP vortex generator shows increment

75.60%, 139.24%, and 143.13% in the coefficient of heat transfer. On the other hand, the maximum percentage of increment at a  $15^\circ$  case with the same Reynolds number was 135.18%, 153.98%, and 154.13%, respectively. The increment in the convective heat transfer coefficient influenced by Reynolds number, shape, angle of attack, and the number of vortex generator usage will also affect pressure drop, which is explained in next part.

### 3.5 Influence of Vortex Generator to the Pressure Drop

A comparison of pressure contour of different VG variation (RWP, CxRWP, CRWP) and without VG is shown in Figure 14.

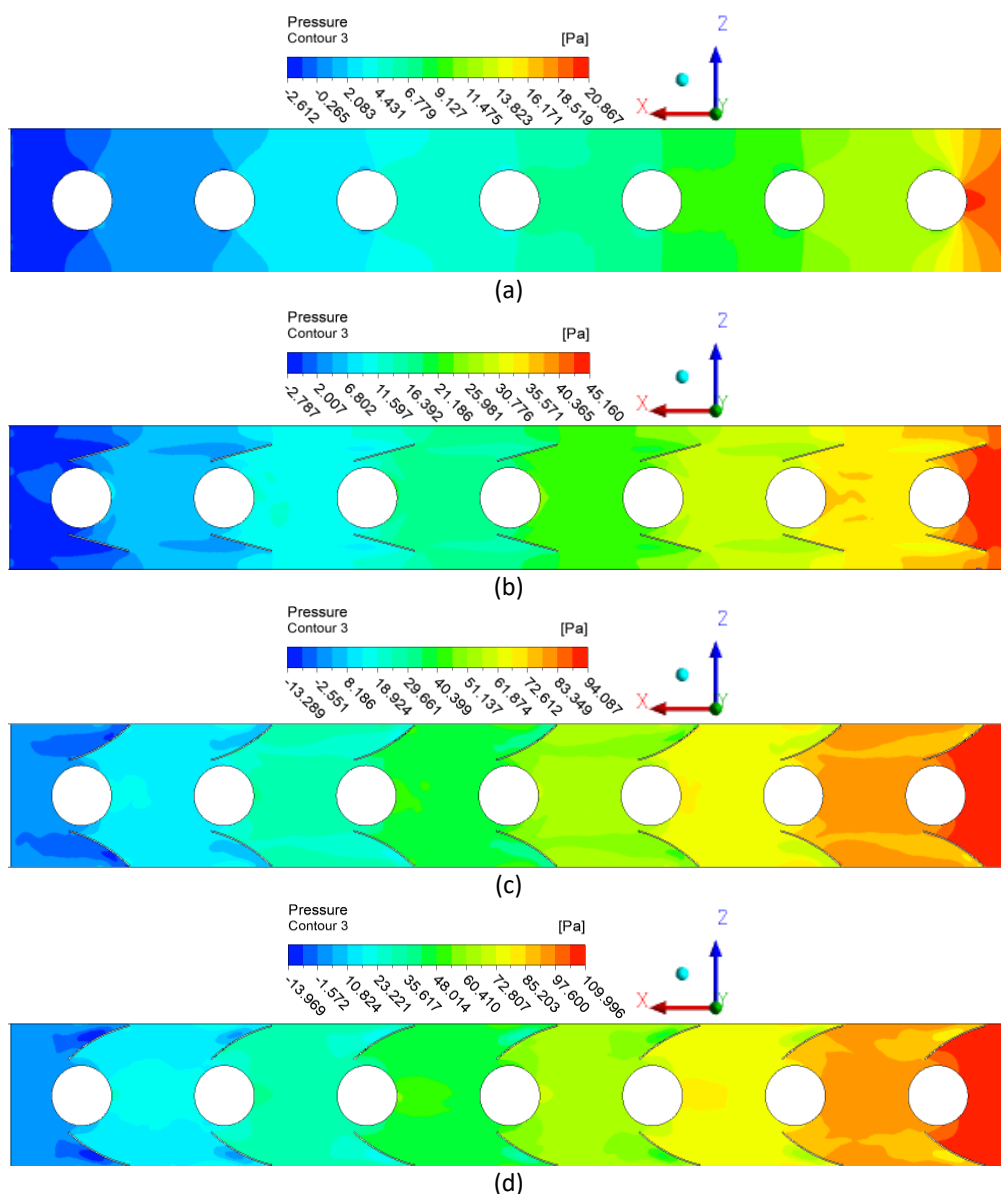


**Fig. 14.** Pressure drop contour: (a) Baseline (b) RWP  $15^\circ$  (c) CxRWP  $15^\circ$  (d) CRWP  $15^\circ$

In Figure 14 above, there is a comparison of the pressure distribution of a  $15^\circ$  case and 662 Reynolds number. The CRWP vortex generator has the highest pressure drop since it has larger frontal area that impedes the mass flow rate. On the other hand, using RWP and CxRWP resulted in a smaller pressure drop than CRWP, leading to less flow deceleration.

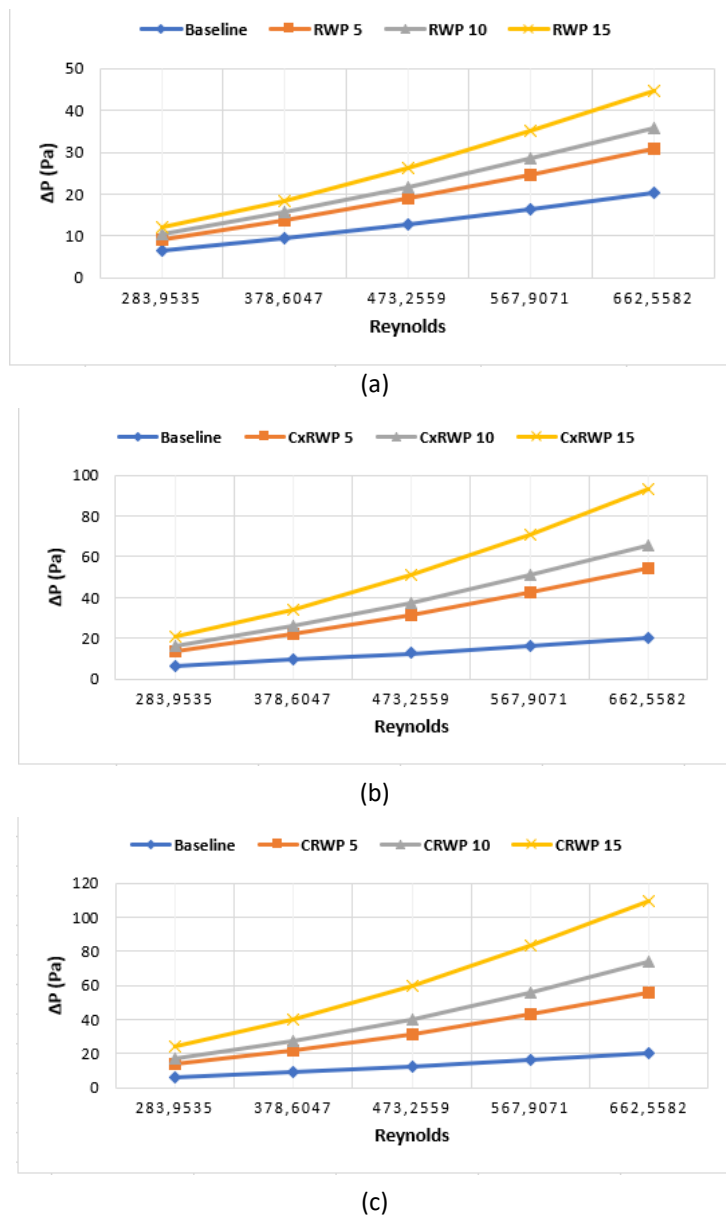


**Fig. 15.** Pressure drop baseline (a) RWP (b) CxRWP (c) CRWP

The pressure drop calculation (refer to Figure 15) is calculated using Eq. (10).

$$\Delta P = P_{in} - P_{out} \tag{10}$$

It is found that the arrangement and shape of the vortex generator affect the pressure drop that occurs due to resistance in the main flow. Pressure drops increases in conjunction of increased Reynolds number. The flow passing through the common flow up arrangement and shape of vortex generators experiences frictional forces on the wall side and resistance in the vortex generator area.

The maximum pressure drops which is 441.30%, occurred on the CRWP type vortex generator at a 15° case and a Reynolds number of 662, while the minimum pressure drop occurs with the RWP vortex generator shape at a 5° case and a Reynolds number of 284, which valued 45.29%.

### 3.6 Influence of Vortex Generator on Heat Transfer

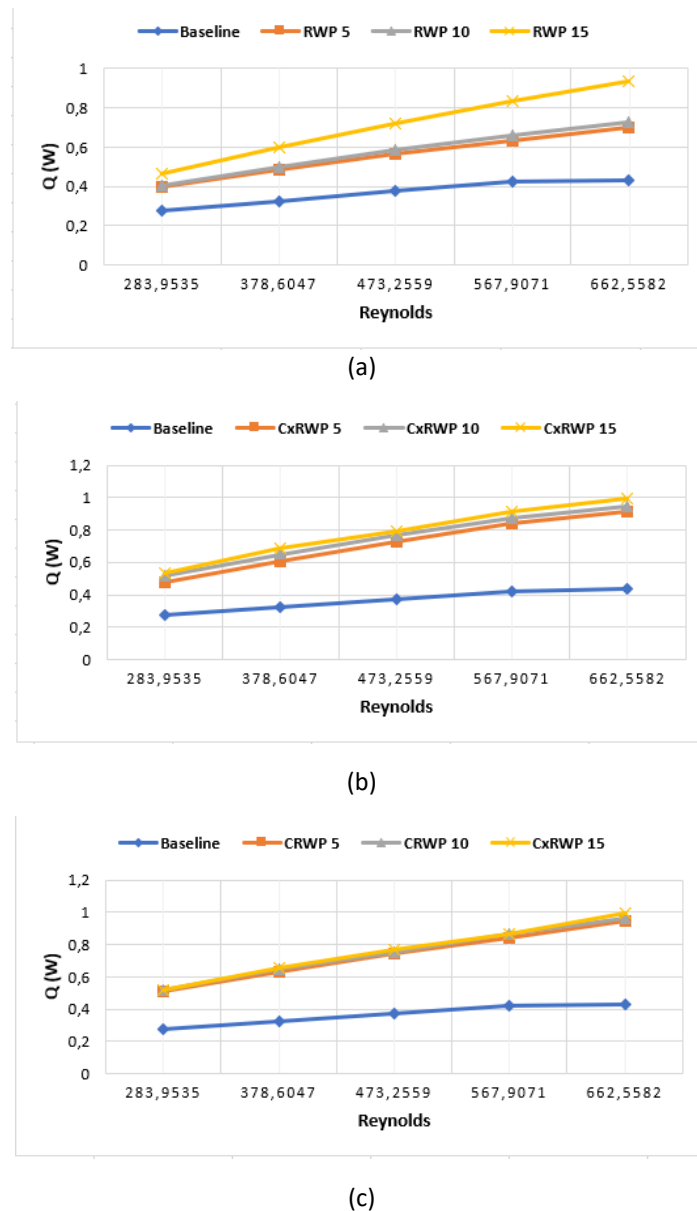


Fig. 16. Heat transfer (a) RWP (b) CxRWP (c) CRWP

Based on the graph in Figure 16, it is evident that a higher value of Reynolds number, geometry, and the angle of attack of the VG in the fin and tube heat exchanger in conjunction with higher heat transfer rate. The graph demonstrates that the heat transfer rate value represents the value of the convective heat transfer coefficient.

## 4. Conclusions

The use of vortex generator variations with increased angles of attack, frontal area, and Reynolds numbers of the vortex generator arrangement can result in better velocity distribution in the flow. The CRWP shape performs 36.08% better in terms of maximum velocity compared to other variations. It can also generate stronger longitudinal vortex intensities, indicated by a 37.65%

increase in maximum velocity compared to other variations. This facilitates fluid mixing in the channel, thinning the thermal boundary layer, and minimizing separation at the backside of the tube.

Vortex generator variations with increased angles of attack, frontal area, and Reynolds numbers of the vortex generator arrangement result in improved temperature distribution in the flow. The CRWP shape performs 1.7699% better at the outlet than the inlet, affecting the convective heat transfer coefficient.

The maximum increment of convective heat transfer coefficient is the CRWP vortex generator with a 15° angle of attack and a Reynolds number of 662 leads to a 154.13% compared to the baseline case. On the other hand, the RWP type VG with 5° angle of attack and a Reynolds number of 284 shows a minimum increment of pressure drop of 45.29% compared to the baseline case.

## Acknowledgement

Thanks to Universitas Sriwijaya to facilities this research.

## References

- [1] Bergman, Theodore L., Adrienne S. Lavine, Frank P. Incropera, and David P. DeWitt. *Introduction to heat transfer*. John Wiley & Sons, 2011.
- [2] Sadeghianjahromi, Ali, and Chi-Chuan Wang. "Heat transfer enhancement in fin-and-tube heat exchangers—A review on different mechanisms." *Renewable and Sustainable Energy Reviews* 137 (2021): 110470. <https://doi.org/10.1016/j.rser.2020.110470>
- [3] Guattari, Claudia, Luca Evangelisti, Paola Gori, and Francesco Asdrubali. "Influence of internal heat sources on thermal resistance evaluation through the heat flow meter method." *Energy and Buildings* 135 (2017): 187-200. <https://doi.org/10.1016/j.enbuild.2016.11.045>
- [4] Awais, Muhammad, and Arafat A. Bhuiyan. "Heat and mass transfer for compact heat exchanger (CHXs) design: A state-of-the-art review." *International Journal of Heat and Mass Transfer* 127 (2018): 359-380. <https://doi.org/10.1016/j.ijheatmasstransfer.2018.08.026>
- [5] Song, KeWei, and Toshio Tagawa. "The optimal arrangement of vortex generators for best heat transfer enhancement in flat-tube-fin heat exchanger." *International Journal of Thermal Sciences* 132 (2018): 355-367. <https://doi.org/10.1016/j.ijthermalsci.2018.06.011>
- [6] Feng, Yongshi, Ruyan Xu, Yi Cao, Xin Wu, Cai Liang, and Liyuan Zhang. "Optimization of H-type finned tube heat exchangers with combinations of longitudinal vortex generator, dimples/protrusions and grooves by Taguchi method." *International Communications in Heat and Mass Transfer* 143 (2023): 106709. <https://doi.org/10.1016/j.icheatmasstransfer.2023.106709>
- [7] Wang, Chi-Chuan, Kuan-Yu Chen, Jane-Sunn Liaw, and Chih-Yung Tseng. "An experimental study of the air-side performance of fin-and-tube heat exchangers having plain, louver, and semi-dimple vortex generator configuration." *International Journal of Heat and Mass Transfer* 80 (2015): 281-287. <https://doi.org/10.1016/j.ijheatmasstransfer.2014.09.030>
- [8] Song, KeWei, and LiangBi Wang. "Effects of longitudinal vortex interaction on periodically developed flow and heat transfer of fin-and-tube heat exchanger." *International Journal of Thermal Sciences* 109 (2016): 206-216. <https://doi.org/10.1016/j.ijthermalsci.2016.06.011>
- [9] Khanjian, Assadour, Charbel Habchi, Serge Russeil, Daniel Bougeard, and Thierry Lemenand. "Effect of rectangular winglet pair roll angle on the heat transfer enhancement in laminar channel flow." *International Journal of Thermal Sciences* 114 (2017): 1-14. <https://doi.org/10.1016/j.ijthermalsci.2016.12.010>
- [10] Liang, G., M. D. Islam, N. Kharoua, and R. Simmons. "Numerical study of heat transfer and flow behavior in a circular tube fitted with varying arrays of winglet vortex generators." *International Journal of Thermal Sciences* 134 (2018): 54-65. <https://doi.org/10.1016/j.ijthermalsci.2018.08.004>
- [11] Awais, Muhammad, and Arafat A. Bhuiyan. "Heat transfer enhancement using different types of vortex generators (VGs): A review on experimental and numerical activities." *Thermal Science and Engineering Progress* 5 (2018): 524-545. <https://doi.org/10.1016/j.tsep.2018.02.007>
- [12] Li, Hung-Yi, Wan-Rong Liao, Tian-Yang Li, and Yan-Zuo Chang. "Application of vortex generators to heat transfer enhancement of a pin-fin heat sink." *International Journal of Heat and Mass Transfer* 112 (2017): 940-949. <https://doi.org/10.1016/j.ijheatmasstransfer.2017.05.032>
- [13] Lu, Gaofeng, and Xiaoqiang Zhai. "Effects of curved vortex generators on the air-side performance of fin-and-tube heat exchangers." *International Journal of Thermal Sciences* 136 (2019): 509-518.

- <https://doi.org/10.1016/j.jjthermalsci.2018.11.009>
- [14] Lei, Yonggang, Fang Zheng, Chongfang Song, and Yongkang Lyu. "Improving the thermal hydraulic performance of a circular tube by using punched delta-winglet vortex generators." *International Journal of Heat and Mass Transfer* 111 (2017): 299-311. <https://doi.org/10.1016/j.ijheatmasstransfer.2017.03.101>
- [15] Joardar, A., and Anthony M. Jacobi. "Heat transfer enhancement by winglet-type vortex generator arrays in compact plain-fin-and-tube heat exchangers." *International journal of refrigeration* 31, no. 1 (2008): 87-97. <https://doi.org/10.1016/j.jjrefrig.2007.04.011>
- [16] J. P. Jean-philipe, T. Vincent, and D. Pierre, "University of Liege Implementation in OpenFOAM of a Melting / Solidification Process with the Enthalpy Method Industrial Tutor : Salvador Lucas," 2017.
- [17] U. Ansys Inc, "Ansys Fluent Theory Guide," *ANSYS Inc., USA*, vol. 15317, no. November, pp. 724–746, 2013.
- [18] Wijaya, Elang Pramudya, Sanjaya Baroar Sakti Nasution, and Agil Fadhel Kurnianto. "Study on the application of particle image velocimetry with resin and rhodamine b as alternative seeding particles in pico hydro cross flow hydro turbine." *Journal of Advanced Research in Fluid Mechanics and Thermal Sciences* 85, no. 1 (2021): 1-11. <https://doi.org/10.37934/arfmts.85.1.111>
- [19] Warjito, Warjito, Budiarmo Budiarmo, Elang Pramudya Wijaya, Kevin Celine, and Sanjaya Baroar Sakti Nasution. "The effect of nozzle-connector angle on cross-flow turbine performance." In *AIP Conference Proceedings*, vol. 2376, no. 1. AIP Publishing, 2021. <https://doi.org/10.1063/5.0063477>
- [20] Arora, Amit, P. M. V. Subbarao, and R. S. Agarwal. "Numerical optimization of location of 'common flow up'delta winglets for inline aligned finned tube heat exchanger." *Applied Thermal Engineering* 82 (2015): 329-340. <https://doi.org/10.1016/j.applthermaleng.2015.02.071>
- [21] Malatesta, Vinicius, Leandro F. Souza, Joseph TC Liu, and Markus J. Kloker. "Heat transfer analysis in a flow over concave wall with primary and secondary instabilities." *Procedia IUTAM* 14 (2015): 487-495. <https://doi.org/10.1016/j.piutam.2015.03.077>
- [22] Naik, Hemant, and Shaligram Tiwari. "Effect of winglet location on performance of fin-tube heat exchangers with inline tube arrangement." *International Journal of Heat and Mass Transfer* 125 (2018): 248-261. <https://doi.org/10.1016/j.ijheatmasstransfer.2018.04.071>
- [23] Syaiful, Syaiful. "Efek Longitudinal Vortex Dihasilkan dari Vortex Generator Jenis Concave Delta dan Rectangular Winglet terhadap Perbaikan Perpindahan Panas: Visualisasi Aliran/Studi Eksperimental." *Jurnal Rekayasa Mesin* 8, no. 3 (2017): 167-173. <https://doi.org/10.21776/ub.jrm.2017.008.03.7>